Journal of the Optical Society of Korea, Vol. 11, No. 1, March 2007, pp. 18-25

Realization of 3-D Topographic and Tomograpic Images with Ultrahigh-resolution Full-field Optical Coherence Tomography

Woo June Choi*, Jihoon Na, Seon Young Ryu, and Byeong Ha Lee

Department of Information and Communications, Gwangju Institute of Science and Technology, 1 Oryong-dong, Buk-gu, Gwangju 500-712, Korea

Dong-Seob Ko

Department of Techno-Marketing, Mokwon University, Daejeon 302-729, Korea

(Received December 12, 2006 : revised March 14, 2007)

We present an ultrahigh-resolution full-field optical coherence tomography (FF-OCT) implemented with a white-light interference microscope and a detector array as an alternative OCT technique. The use of detector array allows the capture of two-dimensional *en-face* images in parallel without taking any lateral scanning process. The phase shifting interferometric technique with the sinusoidal phase modulation (SPM) is utilized to get the demodulated OCT images. The configuration of the system and the resolution of the obtained image are presented. The topographic images, taken with the implemented system, of a coin, an integrated circuit chip, and the tomographic images of an onion epithelium are demonstrated also. Axial and lateral spatial resolution of ~1.0 μm and ~2.0 μm are achieved with the system respectively.

OCIS codes : 170.0170, 170.4500

I. INTRODUCTION

Since optical coherence tomography (OCT) was developed for the first time in 1991 [1], OCT has been widely used as an optical imaging method for medical and biological samples [2-4]. The features of OCT such as sub-micrometer resolution, high detection sensitivity and non-invasive operation together with its ability of imaging a high scattering media made OCT a popular imaging tool compared to the ultrasonic and microwave counterparts. The optical configuration of OCT is usually based on fiber-optic Michelson interferometer. This optical heterodyne detection technique measures the weak light back-scattered from the sample being imaged.

Conventional OCT systems require transverse (X or Y) mechanical scanning over the sample to obtain a cross-sectional image or an *en-face* image. For instance, a time domain OCT (TD-OCT) system acquires the depth profile of a sample by scanning the delay-line (A-scan) and constructs a two-dimensional image by moving the sample stage (B-scan) [1-4], while a frequency domain OCT (FD-OCT) system keeps the reference optical path length fixed and acquires the depth information from the spectrum of the output beam. Although the FD-OCT system avoids A-scan, it still requires B-scan to acquire the cross-sectional image of a sample [5,6]. Mechanical scanning of these OCT systems, however, makes the system slow, cumbersome, and generates artifacts in the image, which results in degradation of the image quality. In addition, use of low numerical aperture (NA) optics also degrades the lateral resolution of the system.

To overcome these drawbacks, full-field optical coherence tomography (FF-OCT) has been proposed as a new alternative OCT method that produces *en-face* tomographic images without lateral scanning and gives a high transverse resolution [7,8]. There are many advantages of FF-OCT. It gives a much higher two-dimensional image acquisition speed compared with existing optical sectioning techniques. Even with an inexpensive broadband light source, a high axial resolution can be obtained. By using high numerical aperture optics, good lateral resolution is possible [7-9].

Usually, FF-OCT system is based on a Linnik-type interferometer, also called as a bulk Michelson interferometer. An incoherent light is illuminated into a Linnik interferometer and split into two arms, the reference arm and the sample arm, of the interferometer. The beams reflected at both arms interfere with each other and the resulted interference pattern is detected by a detector array such as a CCD camera.

In a FF-OCT system, the interferometric signal (coherent signal) is usually very weak compared to the background signal (incoherent signal). To extract the feeble signal of interest (coherent signal) sunk in the interferometric signal, many efforts have been made. Bourquin *et al.* [10] proposed the method based on a two-dimensional smart detector array. Akiba *et al.* [11] presented the heterodyne detection method that needed a pair of CCD cameras. However, the smart detector array method brought out a low lateral resolution and the use of a pair of CCD camera was not cost-effective.

In this paper, we present the phase-shifting interferometry (PSI) technique that can be applicable to a FF-OCT system for retrieving 2-D *en-face* information. The FF-OCT system based on the PSI technique needs only a conventional CCD camera and high NA optics for image acquisition, but it is cost-effectiveness and supports high resolution image. We explain the image acquisition process of the PSI-based FF-OCT, and the resolution of the implemented system is presented and analyzed. The experimentally obtained ultra-high resolution topographic images of a coin, an integrated circuit (IC) chip, and tomographic images of an onion are demonstrated.

II. EXPERIMENTAL SET-UP

The experimental set-up of the FF-OCT system is shown schematically in Fig. 1. It is based on a Linnik-type interferometer [7-9]. An illuminator having a 250 W customized quartz tungsten halogen (QTH) lamp was used as an ultimate incoherent light source. A plano-convex lens L_1 was placed in front of the illuminator for collecting the light from the illuminator. In the reference arm of the interferometer, a silver coated mirror (reflectivity >99%, operated at 650 nm ~ 1050 nm) was used as the reference mirror (RM) and a neutral density (ND) filter was placed to adjust the intensity of the reference beam. The reference mirror was attached to a piezoelectric (PZT) actuator and driven to oscillate at a specified frequency. In the sample arm of the interferometer, a sample was placed on a high precision motorized linear stage having a 0.1 μm resolution to translate the sample position in depth. Two identical microscope dry objective lenses (MO) (20× and 0.45 NA in air) were utilized in both the reference arm and the sample arm.

The beams from both arms were projected at the same time onto a silicon based CCD array (640×480 pixels, 8 bits), thus interference image was expected. A D/A board was used to generate a synchronized signal and to control the exposure time of the CCD camera. Concurrently, a synchronized sinusoidal signal generated by the D/A board drove the PZT actuator for generating a sinusoidal phase modulation. Four interference images were taken over one modulation period of the PZT and used to construct one *en-face* image of the sample. The detailed description and analysis are followed.

III. PROCESS OF IMAGE ACQUISITION

The phase-shifting interferometry (PSI) [12] technique was used in this study to construct an *en-face* image of a sample. The PSI has been employed in almost all types of interferometric imaging systems to extract a phase map from several phase-shifted interference fringe patterns. Among the algorithms used in the literatures to obtain the phase map, we adapted the integrating-bucket technique that was based on the sinusoidal phase modulation (SPM). A CCD camera captured four interference images successively during one period of phase modulation [13,14]. Each CCD image was taken after accumulating for a quarter period. The major advantage of this algorithm is that the phase modulation of the reference beam can be easily performed by using a simple vibrating mirror, such as the mirror attached on a PZT. In addition, the sinusoidal oscillation can be remained steady at a much higher modulation frequency compared to other phase-shifting algorithm based on mechanical displacements [14].

In this section, the principle of the integrating-bucket method with SPM is described. For simplicity, it is assumed that the input beam is monochromatic

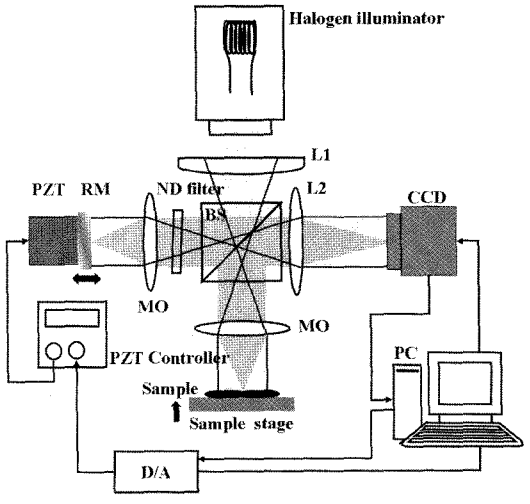

FIG. 1. Schematics of the experimental set-up. The light source is a quartz tungsten halogen (QTH) lamp in an illuminator. BS, beam splitter; ND filter, neutral density filter; MO, microscope objective (dry lens, 20×, 0.45 NA); L#, lenses; RM, reference mirror; PZT, piezoelectric transducer actuator; CCD, charge-coupled device (640× 480 pixel); D/A, digital analogue board.

and a plane wave. Then, the intensity of the interference signal at each CCD pixel located at a designated position (a_x, a_y) across the CCD plane is expressed as [14]

$$I(a_x, a_y) = I_{incoherent}(a_x, a_y) + I_{coherent}\cos\phi(a_x, a_y), \quad (1)$$

where $I_{incoherent}(a_x, a_y)$ is the unwanted background incoherent signal, and $\phi(a_x, a_y)$ is the optical phase difference (OPD) between the object and the reference beams of the interferometer. The intensity of the coherent signal that we want to obtain is denoted as $I_{coherent}(a_x, a_y)$ in the equation.

When the optical path length of the reference arm is sinusoidally modulated, the phase factor of Eq. (1) is modified, which makes the CCD pixel signal become

$$I(a_x, a_y, t) = I_{incoherent}(a_x, a_y) + I_{coherent}\cos[\phi(a_x, a_y) + \psi\sin(\omega t + \theta)], \quad (2)$$

where ψ, θ and ω are the amplitude, the initial phase, and the angular frequency of the modulation, individually. The phase modulation was made in the experiment by vibrating the reference mirror with a PZT as shown with Fig. 1. The initial phase θ is controlled by adjusting the trigger time of the CCD image capture relative to the PZT motion. The time-varying signal $I(a_x, a_y, t)$ is accumulated over one-quarter of the modulation period ($T = 2\pi/\omega$) at the corresponding CCD pixel and then passed to a PC for data storage. Four consecutive signals taken at each quarter period are used to reconstruct the sample image at a point.

The accumulation of the signal at a CCD pixel over a quarter-period is the same as integrating Eq. (2) with respect to time over the same time interval. The consecutive imaging means taking successive integrations over the same intervals but at different starting times. Thus, the four consecutive signals taken at a CCD pixel are mathematically represented as

$$I_n = \frac{T}{4} I_{incoherent} + I_{coherent}\int_{(n-1)T/4}^{nT/4} dt\,\cos[\phi + \psi\sin(\omega t + \theta)]$$
$$\text{for } n = 1, 2, 3, 4 \quad (3)$$

According to the work of Dubois *et al.*, the wanted $I_{coherent}(a_x, a_y)$ is obtained from the accumulated four signals by a simple mathematical manipulation of

$$I_{coherent}^{\ 2} \approx (I_1 - I_2 - I_3 + I_4)^2 + (I_1 - I_2 + I_3 - I_4)^2. \quad (4)$$

It is noteworthy that Eq. (4) holds at a certain combination of the modulation parameters, ψ and ϕ. The detail procedure for getting the optimum modulation parameters can be found in the reference 14. In our experiment, the optimum values of modulation amplitude and the synchronization phase θ were found to be 3.47 and 1.02 (58.5 deg), respectively.

The experimental procedure for extracting the coherent image of a sample was verified by imaging a surface mirror that had some flaws on it. At first, a silver coated mirror was placed at the sample stage with a slight tilt angle and the length of the reference arm was adjusted to give an interference fringe at the CCD. Figure 2 shows the experimental procedures.

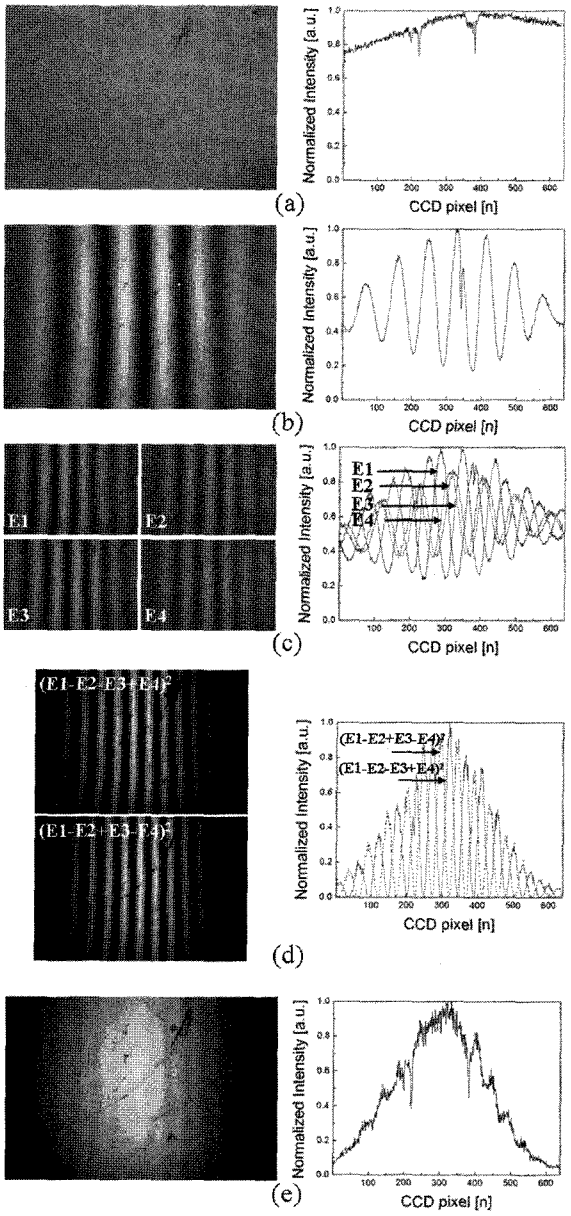

FIG. 2. Experimental procedures for getting coherent image extraction. (a) Microscope image of a tilted mirror. It was taken by simply blocking the reference arm of the system. (b) Interference image taken by the FF-OCT. (c) Four FF-OCT images taken at different phases. (d) Cosine and sine images of the sample obtained by combining the four images of (c). (e) Extracted coherent image. The figures in the right column are the corresponding line images.

Figure 2 (a) was the CCD image of the tilted-mirror taken while blocking the reference beam. Thus, it was just the same as the conventional microscope image of the mirror, which we wanted to reconstruct by using the FF-OCT.

After turning on the reference beam of the interferometer, the CCD image was taken again and depicted at Fig. 2 (b). The image had vertically aligned interference fringes, which means the sample mirror was tilted. The tilting angle of the mirror was adjusted to give a moderate number of interference fringes. As well known, the fringe spacing is inversely proportional to the tilting angle. While oscillating the reference mirror by using a PZT, the optical signal that was accumulated on the CCD during each quarter period of the PZT oscillation was taken. The four accumulated CCD images taken in-series were shown with Fig. 2 (c). By combining these four images properly, two images corresponding to cosine and sine squares of the second term of Eq. (2) were extracted and shown in Fig. 2 (d). Finally, by adding these two images, from Eq. (4), the coherent signal (the fringe envelop signal) of the tilted mirror was obtained and shown with Fig. 2 (e).

We can see that the extracted image of Fig. 2 (e) is well matched, on the whole, with the original microscope image in Fig. 2 (a). However, there are two major mismatches. The first thing is that the original image shows the whole area of the sample, while the extracted image shows only part of it, the central part in this case. In general, the reduction of the imaging area is resulted from the coherent gating property of the FF-OCT; the system shows the area of the sample whose axial position is same as the reference mirror within the coherence length of the light source. However, showing only the central part of the sample, in Fig. 2 (e), strongly forces us to conclude that the optical aberration of the system was so big that the coherent gating effect was overwhelmed. The similar effect can be seen with a coin sample, which will be followed.

The second mismatch is that the extracted image Fig. 2 (e) still has remnant interference fringes, the series of vertical lines in the figure. Even in theory, it is impossible to remove the fringe completely. The best thing is experimentally finding the optimum values of the modulation parameters. In our experiment, the optimum values of the modulation amplitude ψ and the synchronization phase θ were found to be 3.47 and 1.02 (58.5 deg), respectively.

IV. SYSTEM RESOLUTION

1. Axial resolution

The axial resolution of an OCT image system is governed mainly by the coherence length of the illumination source, which is inversely proportional to the spectral bandwidth of the source. Generally, the axial resolution is defined as the full width at half-maximum (FWHM) Δz of an interferometric signal. If we assume the source to have a Gaussian shape spectrum, the axial resolution is given as

$$\Delta z = \frac{\sqrt{2}\ln 2}{n\pi}\left(\frac{\lambda_0^2}{\Delta\lambda}\right) = \frac{L_c}{2n\sqrt{2}} \tag{5}$$

where n, λ_0, $\Delta\lambda$ and L_c are the refractive index of the medium, the center wavelength, the spectrum bandwidth (FWHM) and the coherence length of the source, respectively.

In the experiment, a quartz tungsten halogen (QTH) lamp was used, which had an ultimately broad and rather flat spectrum. However, the CCD array, based on silicon, had a limited spectral bandwidth due to its wavelength dependent responsivity. Thus, the total effective spectral bandwidth of the system was assumed around 330 nm. Figure 3 (a) shows the point spread function (PSF) of the system simulated with Eq. (5). The theoretical axial resolution in air was around 0.5 μm. To get the axial resolution of the system experi-

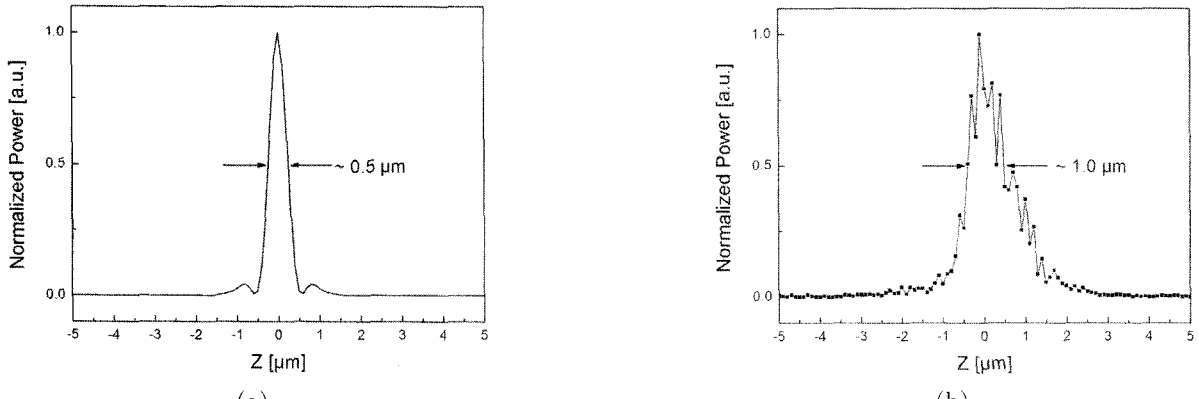

FIG. 3. (a) Numerically simulated axial (z) profile of PSF. (b) Measured axial (z) profile of PSF.

mentally, a stack of tomographic images were obtained by translating the silver coated mirror in the axial (z) direction with a step of 0.1 μm by using a high precision linear motorized stage. Then, the axial (z) intensity profile of the mirror sample was measured by taking the signal from a particular pixel of the CCD. The FWHM of the measured axial profile of PSF was about 1.0 μm. It was rather broader than the theoretical one. The difference between them might be attributed to mainly two factors: the spectral responsivity of the CCD camera might be different from the one supported by the vendor and the shape of system spectrum was too much far from the Gaussian one used for simulation. The dispersion mismatch between two arms of the interferometer might cause appreciable deviation also. The group velocity dispersion induced by the insertion of the ND filter in the reference arm was not compensated in the system. In the experiment, checking the feasibility of the proposed system had the more priority than anything else.

2. Lateral resolution

In a conventional diffraction-limited optical system, the lateral resolution is decided by the Airy function [15]. In the case of a microscope objective lens, the lateral resolution Δx of two just-resolved objects located near the focal plane of the lens is given by

$$\Delta x = f\left(\frac{1.22\lambda}{D}\right) = \frac{1.22\lambda}{NA} \tag{6}$$

where f, D and NA are the focal length, the diameter, and the numerical aperture of the lens, respectively. In the experiment, the NA of the microscope objective lens was 0.45 and the center wavelength of the system was about 700 nm, thus, an effective resolution of 2.0 μm was expected. In practice, the lateral resolution of the system is limited by the pixel size of the CCD camera also. Using the 0.45 NA lens, we could resolve the chrome patterns 7-6 of the 1951 U.S Air Force test target having a width of 3.9 μm, the TLM (Transmission Line Model) patterns of a semiconductor having a width of ~2 μm.

V. SAMPLE IMAGING

Various samples were imaged with the implemented FF-OCT system. At first, the topology image of a coin surface was measured. A one-cent U.S coin shown in the top left-hand corner in Fig. 4 was used. The characters 'ONE', represented by the square in the figure, was imaged. In order to image such a large area of 5.8 mm × 4.7 mm, the objectives lenses at both arms were removed. Before imaging, the actual depth of the coin was measured using a micrometer. The depth from the top surface of the character to the background bottom of the coin was 66 μm. We acquired total 145 images by moving the coin in the z-axis with a step of 0.5 μm by using a high precision motorized linear stage. Figure 4 shows some *en-face* images of the coin measured at several depths. We can see that only a partial surface image of the characters was achieved at the very surface of the coin (see Fig. 4 (a), (b), and (c)). By stacking the *en-face* images of the coin in depth, the three-dimensional volumetric image of the coin was obtained and presented in Fig. 5. The figure shows that the coin itself has a slight curvature. However, much of the curvature might be resulted from the aberration

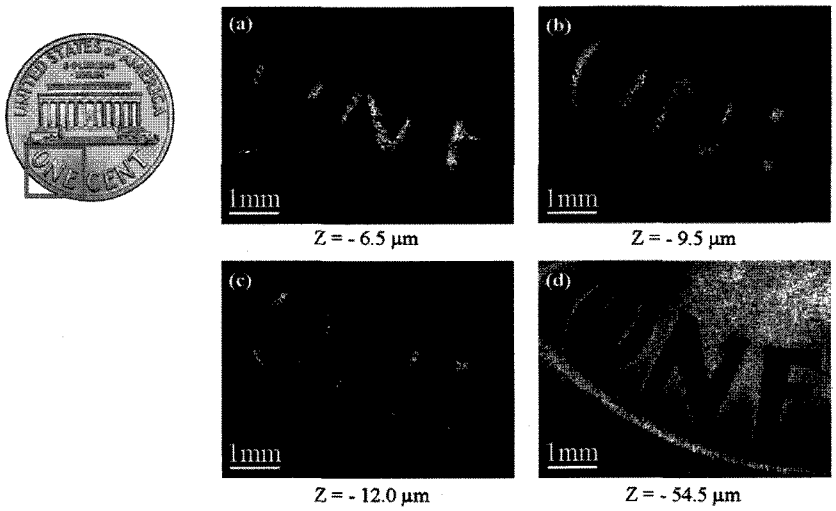

FIG. 4. *En-face* reflectivity images of a one-cent US coin taken at different depths: (a) 6.5 μm, (b) 9.5 μm, (c) 12.0 μm, (d) 54.5 μm, below the surface. The picture at the top on the left-hand corner is a conventional one. The imaged area was 5.8 mm × 4.7 mm as indicated by the square box in the picture.

of the optics in the system as mentioned with Fig. 2 (e) previously. From this image, the height of the characters in the coin was measured as 66.5 μm, which was well matched with the one of 66 μm measured with a micrometer.

As the second sample of the FF-OCT, an integrated circuit (IC) chip having multi-layer structures was chosen. In order to reveal only the metal layers distinctly, the chip was dipped into a BOE (Buffered Oxide Etch) solution for a half an hour. The picture of the IC chip was shown at the top of Fig. 6. Some part within the dotted square box of the picture was topologically imaged. Figure 6 (a) shows the cross-sectional *en-face* images of the chip taken at successive depths with 0.3 μm axial steps. The total number of images were 20, thus, 6 μm scanning was made along the depth of the sample. The acquisition time per each *en-face* image was 2 s. From the figure, we can see that the chip has a complicated topological structure. Each *en-face* image shows different features of the sample. For comparison, the conventional microscope images of the sample were measured at several depths. Six images were taken with 1.8 μm steps and shown with Fig. 6 (b). However, any appreciable change among the images was not observed. In other word, the conventional noninterference microscopy could not discern the topological structure of the IC chip, but the FF OCT could.

The 20 *en-face* images of the IC chip were stacked and formed into a three-dimensional image. Figure 7 (a) and 7 (b) are the same 3-D image but presented in different angles. The three-dimensional structure of

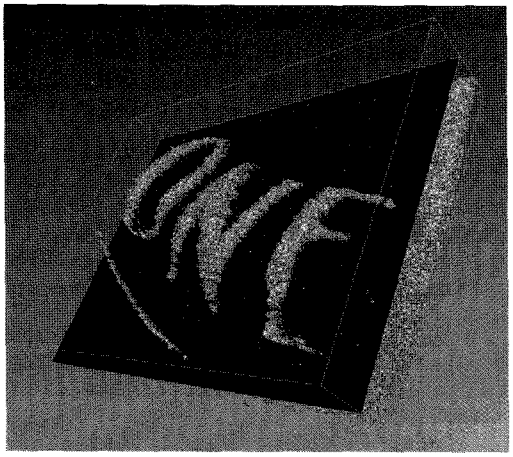

FIG. 5. Constructed three-dimensional topographic image of the one-cent US coin.

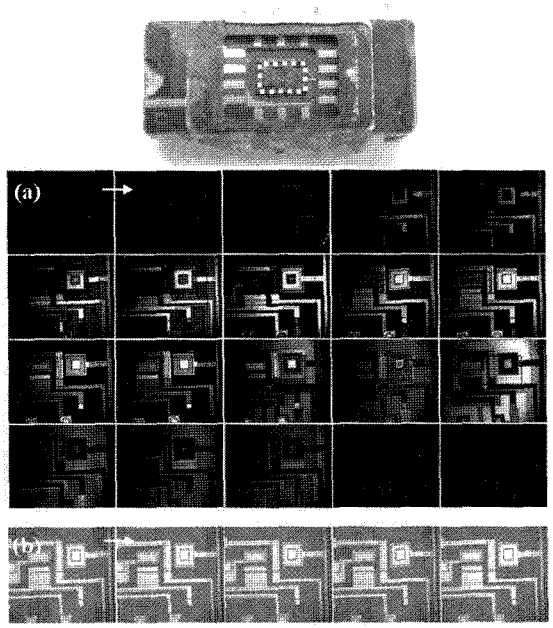

FIG. 6. *En-face* reflectivity images of an integrated circuit (IC) chip taken at every 0.3 μm depths: (a) *En-face* reflectivity images (b) Conventional microscope images taken at every 1.8 μm depths. The picture at the top is the IC chip used for measurement. The dotted square box in the middle (250 μm × 200 μm) is the area where the FF-OCT images were taken.

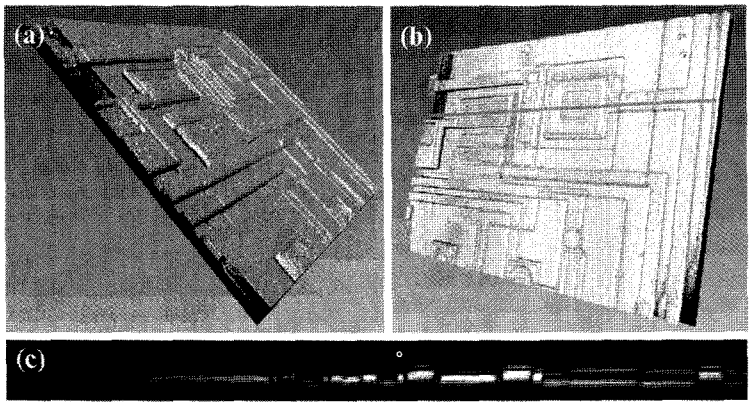

FIG. 7. (a), (b) The constructed three-dimensional topographic images of the integrated circuit chip presented at different angles. (c) Cross-sectional 2-D image of the chip taken along the horizontal line in (b).

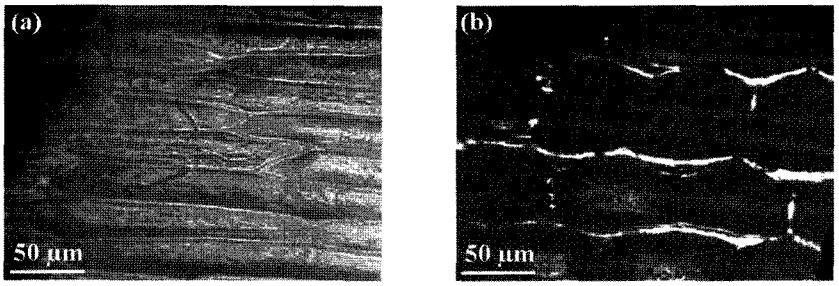

Z = 0 μm Z = -50 μm

FIG. 8. *En-face* tomographic images of an onion epithelium taken at the very surface (left) and at a plane 50 μm below the surface (b). The image size was 250 μm × 200 μm.

the chip is clearly discriminated. One cross-sectional 2-D image of the chip was taken along the horizontal solid line in Fig. 7 (b) and shown with Fig. 7 (c). It clearly shows the depth profile of the chip along the line.

Finally, an onion was used as a biological sample. The tomographic images of an onion epithelium were taken with the implemented FF-OCT. The incident light power upon the sample was 14 μW. Figure 8 shows the *en-face* images of the onion epithelium taken at the very surface and at a plane 50 μm below the surface. The image clearly showed the cell walls and the tissue structures.

The detection sensitivity of the system was measured to be 58 dB without averaging. This sensitivity level is less than other conventional OCT techniques (98 dB with a frequency domain OCT system [16], 85 dB with a high speed scanning *en-face* system [17]). Such a rather low sensitivity of the system is thought to be resulted mainly from the low dynamic range and the poor full-well capacity (FWC) of the CCD camera used for the experiment.

VI. CONCLUSION

We have implemented a full-field optical coherence tomography (FF-OCT) system based on a bulk-optics Linnik-type white light interferometry, which could produce tomographic images without any lateral scanning. The interference signal was detected with a 2-D CCD array. To extract the coherent signal (the fringe envelop signal), the integrated-bucket technique with sinusoidal phase modulation (SPM) was utilized. The optical path length of the reference arm of the system was sinusoidally modulated by using a PZT. The interference signal accumulated in the CCD during a quarter of a modulation period was captured. From the four successively captured images, one *en-face* image could be extracted.

As the white light source, a quartz tungsten halogen (QTH) lamp was used, which enabled us to have a high axial resolution. By using dry microscope objective lenses (0.45 NA) and a neutral density (ND) filter, we could achieve ~1.0 μm axial and ~2.0 μm lateral spatial resolution respectively. With the implemented FF-OCT, we could take the topographic images of a coin, an integrated circuit chip, and the tomographic image of an onion epithelium.

Even though the implemented system showed rather low sensitivity, it supported a high spatial resolution suitable for imaging various biological samples at their cellular levels. The system might be able to find its application where the detailed surface profile of a very fine sample is required. Compared to other optical sectioning systems, the FF-OCT system has the advantage of achieving a high axial resolution with a high image acquisition speed by using an inexpensive white light source.

ACKNOWLEDGMENTS

This work was supported in part by the Korea-China Joint Research Project of Ministry of Science and Technology (MOST), and by Advanced Technology Center (ATC) project of Ministry of Commerce Industry and Energy (MOCIE), and by MOST through the Strategic National R&D program, Korea.

*Corresponding author : leebh@gist.ac.kr

REFERENCES

[1] D. Huang, E. A. Swanson, C. P. Lin, J. S. Schuman, W. G. Stinson, W. Chang, M. R. Hee, T. Flotte, K. Gregory, C. A. Puliafito, and J. G. Fujimoto, "Optical coherence tomography," *Science 254*, pp. 1178-1181, 1991.

[2] J. G. Fujimoto, M. E. Brezinski, G. J. Tearney, S. A. Boppart, B. E. Bouma, M. R. Hee, J. F. Southern, and E. A. Swanson, "Optical biopsy and imaging using optical coherence tomography," *Nat. Med.*, vol. 1, no. 9, pp.

970-972, 1995.

[3] B. Bouma, G. J. Tearney, S. A. Boppart, M. R. Hee, M. E. Brezinski, and J. G. Fujimoto, "High-resolution optical coherence tomographic imaging using a mode-locked Ti:Al_2O_3 laser source," *Opt. Lett.*, vol. 20, no. 13, pp. 1486-1488, 1995.

[4] M. R. Hee, J. A. Izatt, E. A. Swanson, D. Huang, J. S. Schuman, C. P. Lin, C. A. Puliafito, and J. G. Fujimoto, "Optical coherence tomography of the human retina," *Archiv. Ophthalmol.*, vol. 113, no. 3, pp. 325-332, 1995.

[5] R. Leitgeb, C. K. Hitzenberger, and A. F. Fercher, "Performance of fourier domain vs. time domain optical coherence tomography," *Opt. Express*, vol. 11, no. 8, pp. 889-894, 2003.

[6] J. F. de Boer, B. Cense, B. H. Park, M. C. Pierce, G. J. Tearney, and B. E. Bouma, "Improved signal-to-noise ratio in spectral-domain compared with time-domain optical coherence tomography," *Opt. Lett.*, vol. 28, no. 21, pp. 2067-2069, 2003.

[7] A. Dubois, L. Vabre, A. C. Boccara, and E. Beaureparie, "High-resolution full-field optical coherence tomography with a Linnik microscope," *Appl. Opt.*, vol. 41, no. 4, pp. 805-812, 2002.

[8] A. Dubois, K. Grieve, G. Moneron, R. Lecaque, L. Vabre, and C. Boccara, "Ultrahigh-resolution full-field optical coherence tomography," *Appl. Opt.*, vol. 43, no. 14, pp. 2874-2883, 2004.

[9] K. Grieve, A. Dubois, M. Simonutti, M. Paques, J. Sahel, J. F. L. Gargasson, and C. Boccara, "*In vivo* anterior segment imaging in the rat eye with high speed white light full-field optical coherence tomography," *Opt. Express*, vol. 13, no. 16, pp. 6286-6295, 2005.

[10] S. Bourquin, P. Seitz, and R. P. Salathe, "Optical coherence topography based on a two-dimensional smart detector array," *Opt. Lett.*, vol. 26, no. 8, pp. 512-514, 2001.

[11] M. Akiba, K. P. Chan, and N. Tanno, "Full-field optical coherence tomography by two-dimensional heterodyne detection with a pair of CCD cameras," *Opt. Lett.*, vol. 28, no. 10, pp. 816-818, 2003.

[12] D. W. Phillion, "General methods for generating phase-shifting interferometry algorithms," *Appl. Opt.*, vol. 36, no. 31, pp. 8098-8115, 1997.

[13] O. Sasaki and H. Okazaki, "Sinusoidal phase modulating interferometry for surface profile measurement," *Appl. Opt.*, vol. 25, no. 18, pp. 3137-3140, 1986.

[14] A. Dubois, "Phase-map measurements by interferometry with sinusoidal phase modulation and four integrating buckets," *J. Opt, Soc. Am. A*, vol. 18, no. 8, pp. 1972-1979, 2001.

[15] F. L. Pedrotti and S. J. L. S. Pedrotti, Introduction to optics (Prentice Hall, 1993), pp. 323-338.

[16] M. Wojtkowski, V. J. Srinivasan, T. H. Ko, J. G. Fujimoto, A. Kowalczyk, and J. S. Duker, "Ultrahigh-resolution, high-speed, Fourier domain optical coherence tomography and methods for dispersion compensation," *Opt. Express*, vol. 12, no. 11, pp. 2404-2422, 2004.

[17] C. K. Hitzenberger, P. Trost, P. Lo, and Q. Zhou, "Three-dimensional imaging of the human retina by high-speed optical coherence tomgoraphy," *Opt. Express*, vol. 11, no. 21, pp. 2753-2761, 2003.